ANALELE UNIVERSITĂȚII
"EFTIMIE MURGU" REȘIȚA
ANUL XXVI, NR. 1, 2019, ISSN 1453 - 7397

Inteligent control of a visual attention system based on the chalcogenide glass optical fibers

Veturia Chiroiu, Nicoleta Nedelcu, Valeria Mosnegutu

The chalcogenide ternary thin films should provide efficient solutions to develop the color filter-free image sensors for rapid capture of vivid colors detection of the motion images of a scene in the cognitive processes of perception and interpretation of motion. The image sensor consists of a light-sensitive cell having a lower and a higher electrode. The chalcogenide thin film is placed between the electrodes together with an imaging circuit that measures the wavelength and the intensity of the incident light beam. This paper proposes an easy-to-use, visual attention model that use the filter-less color image sensor to a mobile supervising robot able to detect not only the motion but also the intent and the purpose of the motion. The robot oversees the subjects' activities, the motion goals and intentions by exploring the eventually dangerous events that could appear during the motion. The feasibility of the proposed attention model has been demonstrated by simulating an example that tracks the dangerous situations on a volleyball game on a playground.

Keywords: *Chalcogenide ternary thin films, filter-less color image sensors, visual attention model, intelligent control*

1. Introduction

Chalcogenides are known as stable amorphous, quasi-amorphous and crystalline materials with applications in several fields as thermoelectric, optics, medicine, etc., due to their special properties of infrared transmission and high refractive index that can be modified as desired [1].

The chalcogenide glasses transmit longer wavelengths in the infrared region than fluoride glasses and silica. Nowadays there is an increased demand for materials with high level (> 96%) of their transmission index in the visible, in the near-infrared as well as in the mid-infrared spectral ranges.

The chalcogenide glasses applications are based on the high light conductivity of fibers without interacting with the light. The light is not modified by scattering, absorption, and reflections as known, but other processes intervene with potentials for fiber lasers, amplifiers, bright sources, and gratings applications. An important application for medical imaging is the *filterless color image sensor* made from a cell with light sensitivity, a lower and an upper electrodes. The chalcogenide is implemented between the electrodes [2].

The filter-less color image sensor is based on the chalcogenide efficiency in transforming the photoelectric phenomenon. The chalcogenide has a larger band-gap than of silicon (1.1 eV) and it is located at a region where visible ray spectrum is biggest, giving a great photoelectric effect.

The article is organized as follows. Section 2 presents the properties of $Ge_xSb_{20-x}Te_{80}$ alloys with composition $x = 15$, 17 and 19 at.% synthesized from elements with 5N purity (Ge, Sb, Te) by the conventional melt-quenching method. The filter-less color image sensor is described in Section 3. The image sensor is consisting of a light-sensitive cell having a lower and a higher electrode. The chalcogenide thin film is placed between the electrodes together with an imaging circuit that measures the wavelength and the intensity of the incident light beam. The visual attention model is presented in Section 4 and the Conclusions are summarized in Section 5.

2. Properties of chalcogenide ternary thin films

Glassy systems $Ge_xSb_{20-x}Te_{80}$ alloys with composition $x = 15$, 17 and 19 at.%, are synthesized from elements with 5N purity (Ge, Sb, Te) by the conventional melt-quenching method [3-6]. The mixture of the elements with proper weight percent was put in a quartz ampoule which was evacuated down to 10^{-3} Pa. The ampoules were loaded in a rotary furnace and were heated up to 950°C. For obtaining homogeneous melting, the glassy mixture was kept continuously at this temperature for 12h by rotating the furnace. After ending the process, the ampoules were pulled out, and the melts were rapidly cooled down in ice water.

Degassing took place at 10^{-1} Pa, for 12 minutes in the atmosphere of N_2 and during this time, the dome is rotating (about 10 rot/min). This process removes the impurities on the walls from the vacuum deposition installation and on the bulk. At 4×10^{-3} Pa pressure, the heating resistance is coupled, ensuring a temperature of 300^0C in the evaporation chamber while rotating the dome at the speed rotation of 10 rpm. Powder material was evaporated at least 400mA electric current. After evaporation, the samples were measured by VASE ellipsometer-J.A. Woolam. The *ellipsometric's* measurements were recorded in the spectral range UV-VIS-NIR.

Having the experimental data, the optical constants (n and k), are determined. The model contains 2 layers on the quartz substrate (Figure 1), roughness layer / chalcogenic layer / substrate.

The chalcogenide layer was simulated by the General Oscillator method involving the Gauss and Lorentz oscillators. The roughness layer, which is considered a mixture of 50% material (film) and 50% voids (air), was modeled with the Bruggemann's effective medium approximation (B-EMA). The optical constants (n & k) according to wavelength are presents in Figure 2.

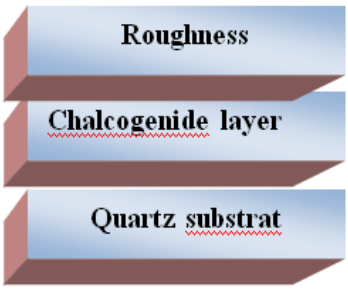

Figure 1. The model layers on the quartz substrate.

According to the Figure 3 the optical constants decreases with the increase the Ge content. The quantity $\alpha(\lambda)$ is given by

$$\alpha(\lambda) = \frac{4\pi k(\lambda)}{\lambda}. \qquad (1)$$

Figure 4 shows the variation of the absorbtion coefficient $\alpha(\lambda)$ with respect to wavelength for $Ge_xSb_{40-x}Se_{60}$ alloys with composition $x = 12$, 25 and 30 at. %.

The optical band gap energy E_g is determined from the absorption coefficient α by using the Tauc's plots for indirect transitions $(\alpha h\nu)^{1/2}$ versus the photon energy $(h\nu)$. The linear part of the Tauc plot is extrapolated at $\alpha = 0$, and the intersection with the energy axis gives the optical band-gaps E_g [7-9].

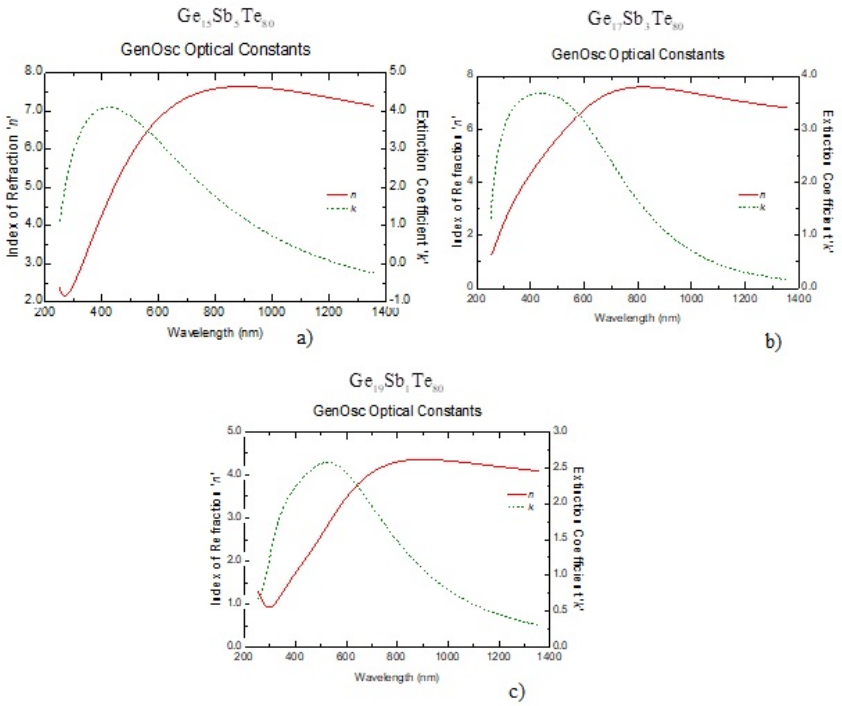

Figure 2. The optical constants (*n* and *k*) for a) $Ge_{15}Sb_5Te_{80}$, b) $Ge_{17}Sb_3Te_{80}$, c) $Ge_{19}Sb_1Te_{80}$

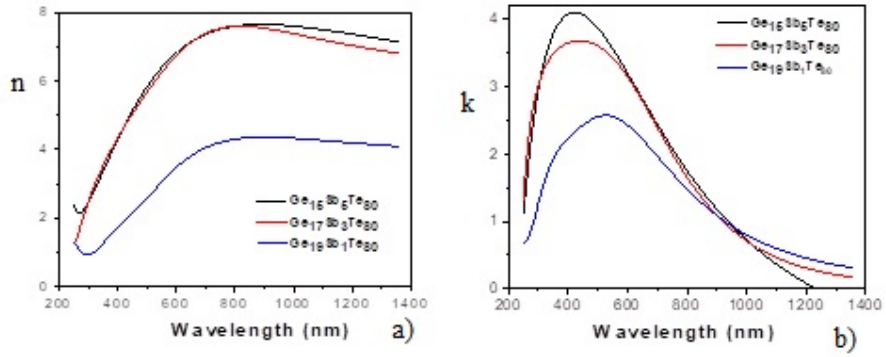

Figure 3. The optical constants n (a) and k (b) for $Ge_xSb_{20-x}Te_{80}$ alloys with composition $x = 15$, 17 and 19 at.%

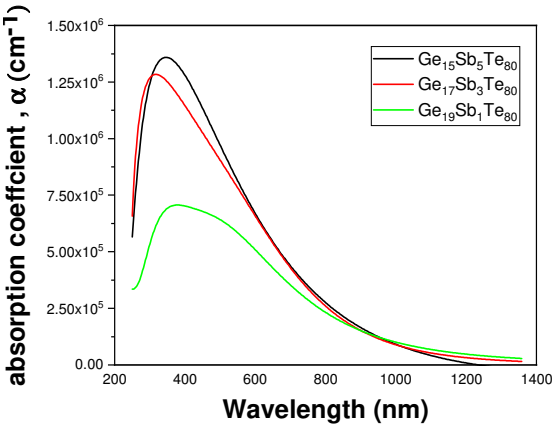

Figure 4. Variation of the absorbtion coefficient $\alpha(\lambda)$ with respect to wavelength for $Ge_xSb_{40-x}Se_{60}$ alloys with composition $x = 12$, 25 and 30 at. %.

3. The filter-less color image sensor

An important application of the chalcogenide thin film is the filterless color image sensor consisting of a light-sensitive cell having a lower and a higher electrode. The chalcogenide thin film is placed between the electrodes together with an image circuit that measures the wavelength and the intensity of the incident light beam. The filter-less color image sensor is presented in Figure 5 [2]. It is consisting from a photo-sensitive cell having a lower electrode, an upper electrode, and a chalcogenide material located between the lower electrode and the upper electrode, an imaging sensing circuit for measuring the wavelength or intensity of incident light based on an electric characteristic value generated from the photo-sensitive cell.

Figure 6 shows the bending of an electron band structure in the photo-sensitive cell after a voltage V_a' is applied to the photo-sensitive cell (the lower electrode $+V_a'$ and the upper electrode 0).

If I_e is the photoelectric current, I_l is the intensity of light, λ is the wavelength of light, and V is the applied voltage, the characteristic curves 1-3 correspond to (Figure 7)

$$V = V_a, I_l = I_{l,0} \ , \tag{2}$$

$$V = V_a' > V_a, I_l = I_{l,0} \ , \tag{3}$$

$$V = V_a, I_l = I'_{l.0} > I_{l.0}\,. \tag{4}$$

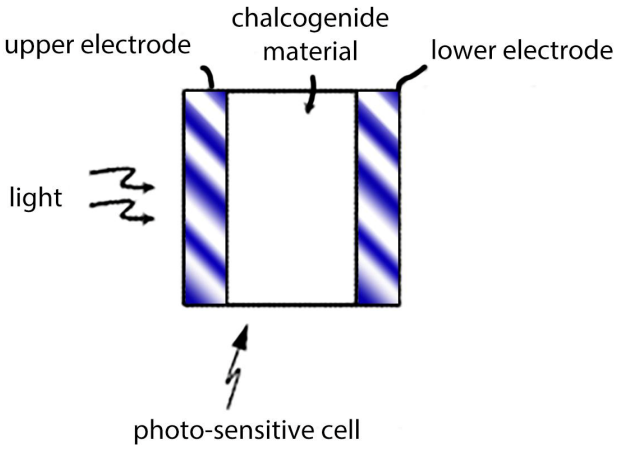

Figure 5. The filteress color image sensor [2].

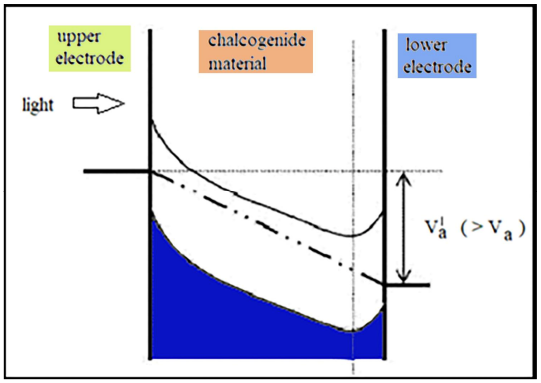

Figure 6. The bending of an electron band structure in the photo-sensitive cell, after a voltage V'_a is applied to the photo-sensitive cell [2].

The visual attention system is composed of a filtered color image sensor implemented in a robotic observer and a visual attention software. The system is learned to adapt to changing conditions and for new tasks.

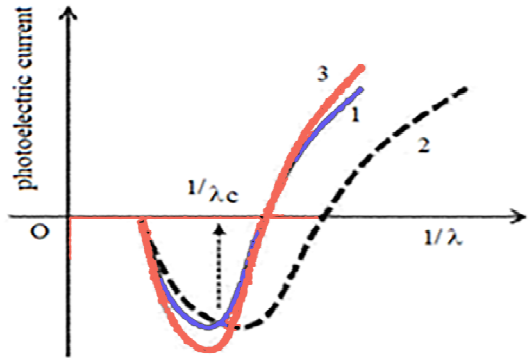

Figure 7. The characteristic curve of photoelectric current [2].

Humans have a great ability to perceive and sense the environment by using rudimentary sensors [10-12]. Animals, birds, and insects excel in making good decisions even if the sensors provide incomplete or incorrect information. The essential idea consists in developing a powerful cognitive tool from communication with peers or from telling stories to each other. The relative positions of the moving objects and the humans are enough for a human observer to understand and make sense of the interaction between humans and objects only by imagining their intentions and goals. This observation must be implemented in the case of a robot observer. Robots occupy many roles reserved for humans. For this reason, the interaction robot-human uses a vision sensorial technique inspired by nature, even if it is a rough approximation of human visual attention.

The cognitive processes of perception and interpretation of motion are related to the computation of physics-based causality and individuation of the objects in motion. Furthermore, the analysis introduces the vectors of attraction and repulsion between humans and objects, in order to explain the causal interactions. The visual attention model is composed of a filtered color image sensor and a visual attention software. The model takes advantage that it receives only rudimentary sensory impressions and uses them to weave a story in which it can take part.

4. Intelligent control of the visual attention model

The optimal control of the visual attention model uses–cell mapping combined with the feedforward supervised artificial neural networks. The simple cell mapping method is based on a discretization of the state-space variables of the system and defining a partition of the state space into cells. The neural controller is presented in Figure 8, and the components of the system, in Figure 8. These components are vision, collision avoidance, self-identification, motion analysis, own goal identification and narrative construction [13-17].

The vision component uses a webcam mounted into the robotic observer. The collision avoidance component is related to the physical dimensions of the space where the robotic observer is moving. If the robot gets too close to the walls or other objects or people, an emergency goal vector pointing straight out will guide it to stop it or to change the direction of movement. The self-identification component is related to the inspection of the visual field by the robot observer, to identify itself and other people engaged in the game.

The motion analysis component observes the behavior of the players. Given a human, the robot follows the motion of others humans who participate in the game in order to start working the rules of the game. For each of the other two subjects, the robot calculates the influence of the remaining subjects (including itself) on the first subject

$$v_{x_i^t} = \frac{c_{x_j}(x_j^t - x_i^t)}{d_{ij}^t} + \frac{c_{x_k}(x_k^t - x_k^t)}{d_{ik}^t}, \tag{5}$$

where $v_{x_i^n}$ is the velocity of the subject i at time t, and d_{ij}^t is the Euclidean distance between the subject i and the subject j.

The own goal identification component describes the influence of one player on the motion of another player during the game. The relationships between players represent essential information that describe attraction and repulsion between them or between people and objects.

At any particular point in time, any player may be attracted or repelled or remain neutral with respect to other players or to some objects. The players remain in a particular intentional state as long as the hypothesis related to attractions, repulsions, and neutralities remain unchanged.

In observing the players motion, this component develops a belief distribution of their possible intentional states. It is able to probe the player's states, to confirm or reject the hypothesis. This component adjusts the beliefs state as times as needed.

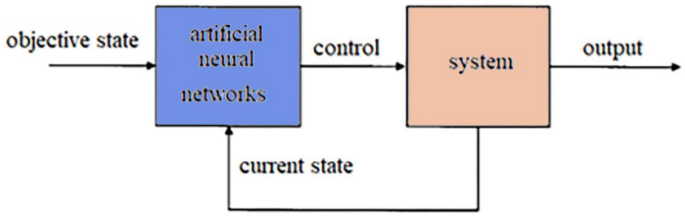

Figure 8. Neural controler [15].

The narrative construction component converts velocity vectors into sustained beliefs about the intentional situation during a particular time of the game. The sequence of states can be interpreted as a narrative describing the game in progress. This narrative construction is able to identify the motion in progress and to detect important points in time where important events take place.

The component observes the relative positions of the players during the crucial moments of a changed state by calculating the distance between players or distance between players and objects.

The filters are modeled as the sum of two Gaussians and the transmittance of spectral sensitivity at each wavelength is smooth and non-negative and does not exceed one.

The cell-to-cell mapping in the optimization flow shown in Figure 9 can be derived from the evolution of the system, so that the system dynamics can be efficiently characterized and analyzed via such mapping.

Optimal simulations were carried out employing the following the state-space equation

$$I_e = f(I_l, \lambda, V), \tag{7}$$

where I_e is the photoelectric current, I_l is the intensity of light, λ is the wavelength of light, and V is the applied voltage. Since I_l is expected as increasing the intensity of I_e in the entire wavelength region, (7) can be rewritten as

$$I_e = g(I_l)h(\lambda, V), \tag{8}$$

$$I_e(V_a) = g(I_l)h(\lambda, V_a), \tag{9}$$

$$I_e(V_a') = g(I_l)h(\lambda, V_a'), \tag{10}$$

where the functions $g(I_l)$ and $h(\lambda, V)$ are unknown. The functions $I_e(V_a)$ and $I_e(V_a')$ can be experimentally measured.

So, determining of $g(I_l)$ and $h(\lambda, V)$ is the key in the optimal control of the visual attention model.

Figure 10 shows the optimal dimensionless function $g = g / g_0$, with g_0 a reference function as a function of light intensity. The optimal dimensionless function $h = h / h_0$, with h_0 a reference function as a function of the wavelength and the applied voltage, is presented in Figure 11.

We tested the visual attention model and its ability to detect the dangerous situations on a volleyball game that involved six kids on a given playground (Figure 12) [18, 19].

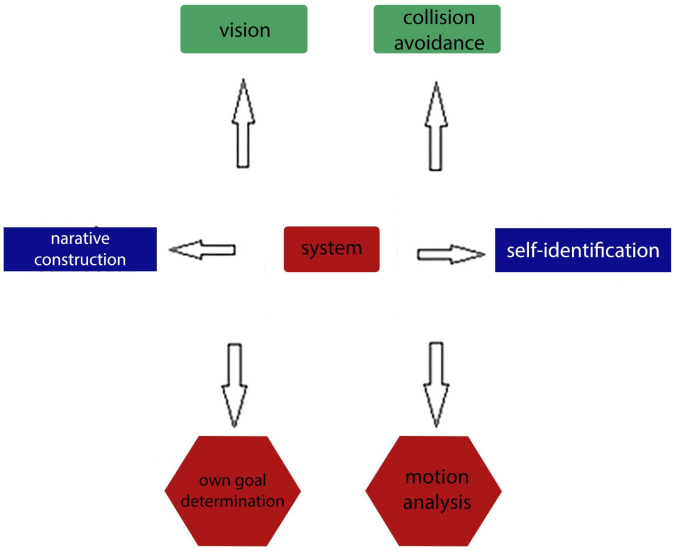

Figure 9. The system.

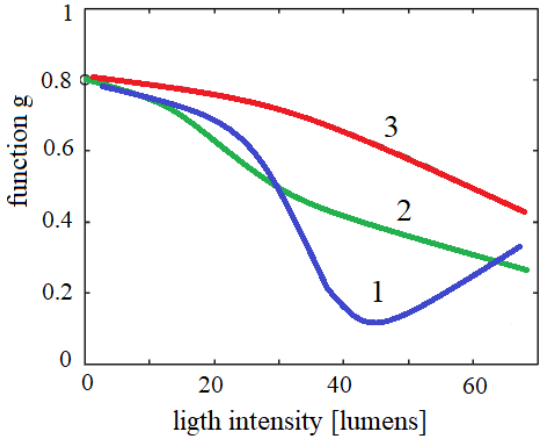

Figure 10. Optimal dimensionless function $g = g / g_0$, with g_0 a reference function as a function of light intensity.

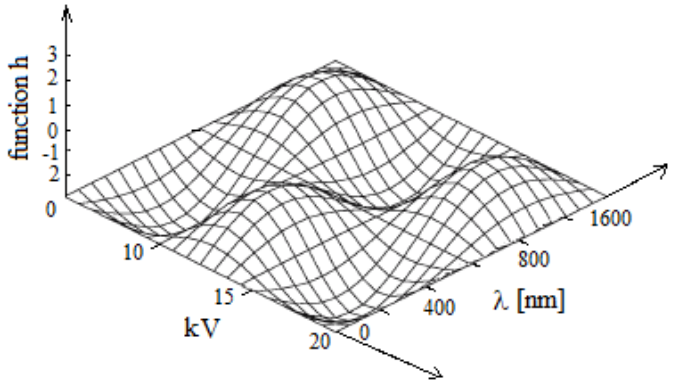

Figure 11. Optimal dimensionless function $h = h / h_0$, with h_0 a reference function as a function of the wavelength and the applied voltage.

The Wolfe's model of visual search and attention is applied in this paper [18]. The robot produces a map of attention through a weighted combination of observations given by various detectors $(s_1,...,s_n)$ (color, motion and shape). This combination allows the robot to select the regions of interest and then, it directs the computer to these regions. The attention system is based on the stimulus-adapting mechanism and runs all the time. The correlation between two different sets of visual data is measured by the correlation coefficient. The correlation coefficient $-1 \le r \le 1$, for k sets of data $(s_1^1, s_2^1, ...s_n^1) ... (s_1^k, s_2^k, ...s_n^k)$ is calculated by

$$r = \frac{\sum_{i=1}^{k}\sum_{j=1}^{n} (s_j^i - \overline{s}^i)}{\sqrt{\sum_{i=1}^{k}\sum_{j=1}^{n} (s_j^i - \overline{s}^i)^2}}, \tag{11}$$

where $\overline{s}^i$ are the mean value of the i- set of data. For $-0.5 \le r \le 0.5$, a little correlation is observed, while for $-0.8 \le r \le 0.8$ we have a strong correlation.

Within less than a second, the system is alerted because it observes the intentional states of two kids -a boy with a mauve undershirt and a girl with black hear, with respect to each other. Then, the system acted and within ~~a~~ five seconds intervene. Figure 12 shows the incidents with the boy and the girl, in the case of no control.

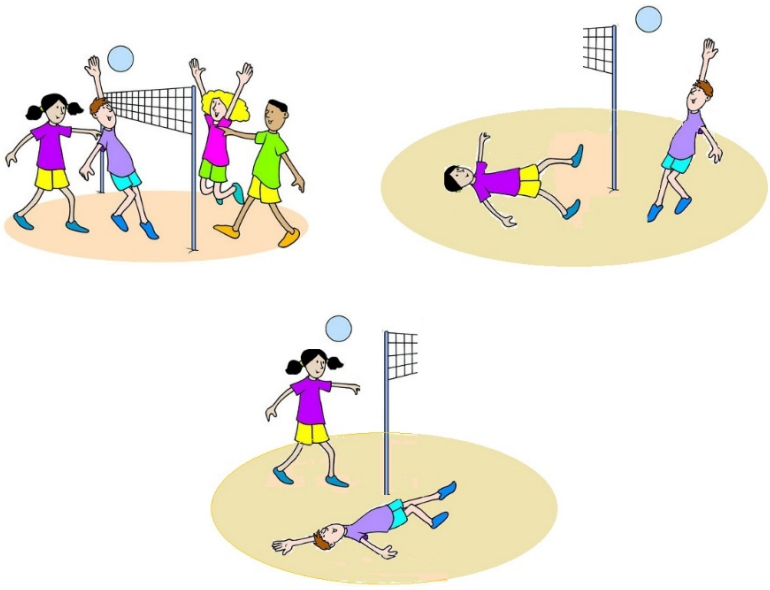

Figure 12. Two incidents with a boy and a girl during the game [19].

7. Conclusion

The optical characteristics of $Ge_xSb_{40-x}Se_{60}$ alloys with composition $x = 12$, 25 and 30 at.%, synthesized from elements with 5N purity (Ge, Sb, Se) by the conventional melt-quenching method, are presented together with their applications as sensors.

A special application is the filterless color image sensor consisting of a light-sensitive cell having a lower and a higher electrode. The chalcogenide thin film is placed between the electrodes together with an imaging circuit that measures the wavelength and the intensity of the incident light beam.

The visual attention model uses the filterless color image sensor combined with visual attention software. Intelligent control of the visual attention model is based on the cell mapping combined with the feedforward supervised artificial neural networks.

The characteristic of the vision sensorial technique are:

1. The vision sensorial system works in principle as a fundamental cognitive, perception, interpretation of the motion and individualization of subconscious moving in the context of causal perceptions;

2. The vision sensorial system works to identify the points of interest in a visual flow;

3. The vision sensorial system data permit the robot to be able to interpret these data in order to achieve a task, to adapt to changing conditions and to learn new tasks.

Acknowledgment. This work was supported by a grant of the Romanian Ministry of Research and Innovation, CCCDI-UEFISCDI, project number PN-III-P1-1.2-PCCDI-2017-0221/ 59PCCDI/2018 (IMPROVE), within PNCDI III.

References

[1] Musgraves J.D., Danto S., Richardson K., *Chalcogenide Glass Thin Film and Fiber Structures for Chemical and Biological Sensing*, Univ. of Delaware, 2012**.**

[2] Su Youn Lee, Byung Ki Cheong, Doo Seok Jeong, https://www.google.com/patents/US9252181

[3] Nedelcu N., Chiroiu V., Rugina C., Munteanu L., Ioan R., Girip I., *Preparation of GeSbSe thin films by conventional melt-quenching method and studying their caracteristic* (in press) 2019.

[4] Dulgheru N., Stoica M., Calderon-Moreno J.M., Anastasescu M., Nicolescu M., Stroescu H., Atkinson I., Stanculescu I., Szekeres A., Gartner M., *Optical, morphological and durability studies of quaternary chalcogenide Ge-Sb(As)-(S,Te) films*, Materials Research Bulletin, 106, 2018, pp. 234–242.

[5] Dulgheru (Nedelcu) N.,Gartner M., Anastasescu M., Nicolescu M., Stoica M., Stroescu H., Atkinson I., Bratan V., Stanculescu I., Szekeres A., Terziyska P., Fabian M., *Influence of compositional variation on the optical and morphological properties of Ge-Sb-Se films for optoelectronics application,* Infrared Physics and Technology, 93, 2018, pp. 260-270.

[6] Fabian M., Dulgheru N., Antonova K., Szekeres A., Gartner M., *Investigation of the Atomic Structure of Ge-Sb-Se Chalcogenide Glasses*, Advances in Condensed Matter Physics, 2018, Article ID 7158079.

[7] Dulgheru (Nedelcu), N., Anastasescu M., Nicolescu M., Stoica M., Gartner M., Pamukchieva V., Szekeres A., Todorova K., *Surface topography and optical properties of Ge-Sb(As)-S-Te thin films by atomic-force microscopy and variable angle spectroscopic ellipsometry*, Journal of Physics: Conference Series, 356, 012019, 2012.

[8] Dulgheru (Nedelcu) N., *Correlation of optical and morph-structural properties in chalcogenide compounds with applications in optoelectronics*, Romanian Academy "Ilie Murgulescu" Institute of Physical Chemistry, 2019.

[9] Tauc J., *Amorphous and Liquid Semiconductors*, Plenum Press, London, 1974.

[10] Scassellati B., *Theory of mind for a humanoid robot*, Autonomous Robots, 12, 13-24, 2002.
[11] Crick C., Scassellati B., *Controlling a robot with intention derived from motion*, Topics in Cognitive Science, 2, 2010, pp. 114-126.
[12] Breazeal C., Scassellati B., *A context-dependent attention system for a social robot*. In Proceedings of the Sixteenth International Joint Conference on Artificial Intelligence, T. Dean (Ed.), 1999.
[13] Crick C., Scassellati B., *Controlling a robot with intention derived from motion*, Topics in Cognitive Science, 2, 2010, pp. 114-126.
[14] Marin T.M., Zufiria P.J., *Optimal control of non-linear systems through hybrid cell-mapping/artificial-neural-networks techniques*, Int. J. Adapt. Control Signal Process, 13, 1999, pp. 307-319.
[15] Lewis F. L., *Optimal Control*, Wiley, New York, 1986.
[16] Hsu C.S., *Cell-to-cell mapping*: *A method of global analysis of dynamical systems*, Springer, New York, 1987.
[17] Hsu C.S., Guttalu R.S., *An unravelling algorithm for global analysis of dynamical systems: an application of cell-to-cell mapping*, J. Appl. Mech., 47, 1980, pp. 940-948.
[18] Wolfe J.M., *Guided Search 2.0: A Revised Model of Visual Search*, Psychonomic Bull. & Rev.,1(2), 1994, pp. 202–238.
[19] Munteanu L., Rugină C., Dragne C., Chiroiu V., *On the robotic control based on interactive activities of subjects,* Proceedings of the Romanian Academy, series A, 2019 (in press).

Addresses:

- Dr.Veturia Chiroiu, Institute of Solid Mechanics, Romanian Academy, C-tin Mille 15, Bucharest, 010141, veturiachiroiu@yahoo.com
- Dr.Nicoleta Nedelcu, Institute of Solid Mechanics, Romanian Academy, C-tin Mille 15, Bucharest, 010141, nicoleta_dulgheru@yahoo.com
- Dr.Valeria Mosnegutu, Institute of Solid Mechanics, Romanian Academy, C-tin Mille 15, Bucharest, 010141, valeriam732000@yahoo.com